International Journal of Modern Manufacturing Technologies
ISSN 2067–3604, Vol.XII, No. 2 / 2020

LASER WELDED S355 AND 316L STEEL PIPE JOINT HYDROSTATIC TEST SIMULATION

Bernard Wyględacz, Tomasz Kik, Marcin Żuk

Silesian University of Technology, Department of Welding Engineering, Konarskiego, No. 18A, 44-100, Gliwice, Poland

Corresponding author: Bernard Wyględacz, bernard.wygledacz@polsl.pl

Abstract: In this article effect of external stress, in form of pressure on inner pipe surface, application on laser welded S355 and 316L steel pipe joints were simulated. Simulations resulted in stressesdistribution before, during and after hydrostatic test. Test pressures were calculated according to Der Norske Veritas (DNV) Rules and Standards for Classification of Ships Part 4, moreover based on analytical calculation higher experimental test pressures were proposed, simulated and compared to DNV Standards test pressure to provide further decrease residual stresses in welded joint. Difference in development of residual and working stress after hydrostatic test for low alloyed C-Mn steel (S355) and austenitic stainless steel (316L) are shown. Simulation results shows high local stress level caused by LBW in the joints. The stress level is further increased by pressure application, but can can be reduced by hydrostatic test application. The stress reduction is dependant on hydrostic test pressure. With increased hydrostatic test pressure plastic distorstion increases slightly,

Key words: FEM, numeric simulation, hydrostatic test, laser welding, stresses distribution.

1. INTRODUCTION

Hydrostatic tests have important place in verification and preparation for exploitation of liquid media bearing installations. When installation is subjected to pressure higher that nominal, not only it is proven free of major manufacturing defects and fit for exploitation, but also manufacturing stress fields are superimposed on stress fields similar to working conditions, which results in plastic deformation and reduction of residual stresses. Application of stress relieving strain under professional supervision ensures detection of structure failure symptoms, if they were to occur [1,2]. In welded joints manufacturing stresses locally reach elastic limit, but it is impossible to determine stress field distribution in welded joint by means of analytical calculation due to shear number of factors e.g.: heat flow during and after welding, non-uniform metallurgical transformations, strain hardening etc. [1-3].

Access to huge computing power resources today allows us to look more boldly towards applications of computational methods in very complex numerical analyzes. This is necessary because the technological development also causes a reach for more and more advanced construction materials. On the other hand, we are boldly designing large, complicated constructions, where often finding the mutual influence of many parameters of the manufacturing process is impossible to obtain by classical computational methods or based on even many years of experience and engineering knowledge [3-7].

In this situation, advanced programs for numerical analysis of technological processes, based on the finite element method, come to the aid. Numerical analyzes of welding processes are currently very modern and at the same time an efficient tool supporting the work of engineers. However, these are also the most complex issues requiring broad and reliable knowledge both in the field of computational methods and technology as well as material issues [4-9].

In recent years approach of finite element method (FEM) numerical computations enabled determination of stresses and distortion fields and metallurgical phase composition in welded joints. To achieve highest convergence and precision in welding simulation, transient non-linear FEM calculation on 3D mesh are needed. Non-linear 3D transient FEM calculations were proven as excellent tool for stresses and distortion prediction in welded joints [8-11].

2. METHODS AND EXPERIMENTAL

In this article welding and hydrostatic testing process of S355 and 316L steel pipes 70 mm in diameter 4 mm thick joints was simulated by FEM in VisualWeld (SYSWELD code). Non-uniform 3D mesh of 49433 elements and 40605 nodes with higher density around welded joint was prepared.

Laser welding was chosen as a simulated method of manufacturing due to increasing popularity in

industry. High residual stresses in laser welded joints are effect of highly concentrated heat source and high cooling rates compared to conventional arc welding methods (GMA, TIG, MMA). Highly variable combined von Misses stresses levels, with maximal values often over 500 MPa for S355 steel joints. Metallurgical transformations, localized in the welded joint, increasing elastic limit and asynchronous sharp thermal cycles along the welded seam can lead to crack formation when residual stresses and nominal stresses overlap.

Simulated case is similar welding and as such calculation of one side of the joint with symmetry condition applied can be used. Boundary conditions were: symmetry condition on welded joint butt surface, elastic clamping on all nodes from other end and free heat exchange on all outer model surfaces with air temperature of 20°C. Laser beam heat source was simulated by 3D conical heat source with modified load elements. 3D conical heat source is most used method in modeling of high energy density beam welding (laser and electron beam welding). Heat source model and parameters are visible in Figure 1.

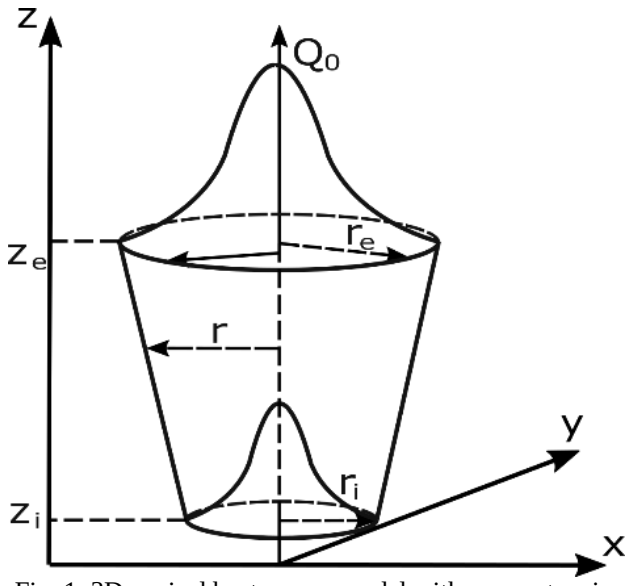

Fig. 1. 3D conical heat source model with parameters in local coordinate system

Conical heat source is described in local coordinates by equation 1 and 2:

$$Q(x,y,z) = Q_0 exp\left(-\frac{x^2+y^2}{r_0^2(z)}\right), \quad (1)$$

$$r_0^2(z) = r_e + \frac{r_i - r_e}{z_i - z_e}(z - z_e), \quad (2)$$

where:

Q_0 – heat flux density [W/m^2],

r_e, r_i – 3D cone radius dimensions parameters [mm],

z_e, z_i – 3D cone length parameters [mm].

During pre-processing local coordinates are translated to global coordinates according to welding speed, heat flux is applied only to nodes contained in collector "welding load" and q_o is matched so linear energy of welding is retained. Changing welding load enables additional method of controlling heat input into model. For simulation of specific shape of fused zone proposal of modified thermal load is tested for 316L steel. The modified load elements are visible as a darker zone in Figure 2. The location and size of the thermal load zone interacts with heat source changing the heat input characteristics into the model during the simulated laser welding [12-14]. The parameters of the heat source model used in the calculations were selected as a result of the calibration of the model and presented in Table 1.

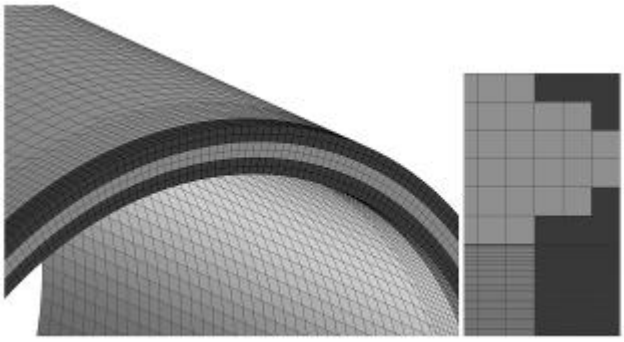

Fig. 2. Welding load (dark elements) for 316L steel numerical simulation

Table 1. Welding simulation parameters and dimensions of 3D conical heat source model

Simulation title	Material database	Welding speed [mm/s]	Linear energy [J/mm]	Efficiency	Heat source top radius r_e [mm]	Heat source bottom diameter r_i [mm]	Heat source height $z_e - z_i$ [mm]
S355_1 … 4	S355	33.33	49.55	0.8	0.74	0.6	4
316L_1 … 4	316L	8.33	90	0.85	1.1	0.9	4

Welding parameters were based on experimental data and thermal fields during welding simulation were compared to macrographs of welded seams to optimize heat source parameters. As only half of model was simulated linear energy of welding must also be divided by two. Time of 2000 seconds was set to allow dissipation of heat introduced to elements. Then additional boundary conditions in form of pressure on inner welded joint surface (Figure 3) was introduced.

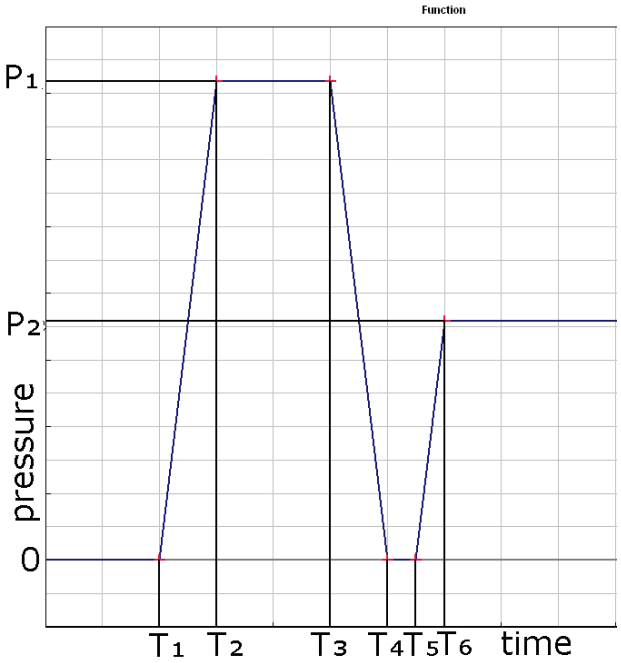

Fig. 3. Pressure function shape and parameters, see Table 2

Pressure is applied to each 2D element of inner pipe surface according to local Z axis, normal to the element surface. The pressure value is applied in form of function, shown in Figure 3, with parameters presented in Table 2. The pressure function has 6 distinct times: T_1 – Start time of test pressure application, T_2 – Time of achieving full test pressure, T_3 – Start time for release of test pressure, T_4 – Time of total release from test pressure, T_5 – Start time of working pressure application, T_6 – Time of achieving full working pressure. The times where chosen to decrease change rate in mechanical calculations. Function has two stress levels where level P_1 is simulated hydrostatic test and level P_2 is meant to present simulated working conditions and is equal to 75% on maximal permitted working pressure according to Det Norske Veritas (DNV) Rules for Classification of Ships Part 4 Chapter 6 and 7 [15]. According to DNV Ship Building Rules testing pressures are 150% of nominal working pressure. Maximal working pressure of 23.9 MPa (239 bar) for S355 steel and 12.5 MPa (125 bar) for 316L steel was calculated according to DNV Ship classification. Analytically calculated pressure corresponding to stress level equal to material yield strength $Rp_{0.2}$ was 45.8 MPa (458 bar) for S355 steel and 31 MPa (310 bar) for 316L steel. That pressure and 105% of that pressure were set as test pressures for round 3 and 4 of computation.

Table 2. Pressure function parameters used in simulations

Simulation title	P_1 [bar]	P_2 [bar]	T_1 [s]	T_2 [s]	T_3 [s]	T_4 [s]	T_5 [s]	T_6 [s]
S355_1	358.5	179.25	2000	2050	2150	2200	2225	2250
S355_2	0							
S355_3	458							
S355_4	480.9							
316L_1	187.5	93.75						
316L_2	0							
316L_3	310							
316L_4	325.5							

Table 3. Minimal and maximal von Mises stresses values

Simulation Title	After welding [MPa]	Test pressure [MPa]	After test [MPa]	Working condition [MPa]
S355_1	min. 0	min. 137	min. 0	min. 40
		max. 813	max. 629	max. 712
S355_2		----		min. 39
				max. 780
S355_3	max 739	min. 226	min. 0	min. 49
		max. 825	max. 575	max. 663
S355_4		min. 250	min. 0	min. 0
		max. 826	max. 559	max. 648
316L_1	min. 0	min. 42	min. 0	min. 11
		max. 375	max. 242	max. 307
316L_2		----		min. 15
				max. 374
316L_3	max. 360	min. 250	min. 3	min. 59
		max. 397	max. 138	max. 211
316L_4		min. 271	min. 3	min. 63
		max. 403	max. 122	max. 198

3. RESULTS AND DISCUSSION

Thermo-metallurgical calculations were completed successfully with correct heat source fitting evidenced by shape of simulated molten metal pool (Figure 4) corresponding with shape of fused zone in macrographical cross-sections of real world welded joints.

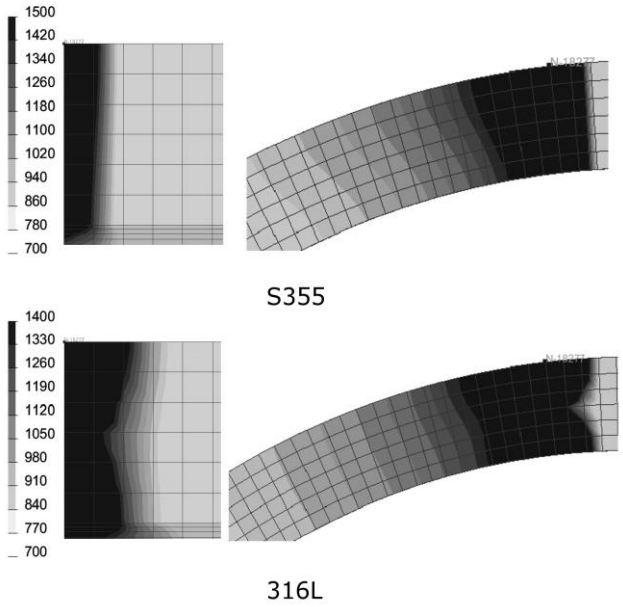

Fig 4. Views of stabilized molten metal pool shape in transverse and longitudinal cross-section.

Mechanical calculations produced result file of around 12 GB for each calculated simulation. During post processing color maps of von Mises combined mechanical stresses distribution for significant time cards were generated. In Figures 5 and 6 whole simulated model surface before during and after hydrostatic testing and simulated working conditions are visible. In the upper left corner of the above-mentioned figures surface stress distribution after welding and cooling to room temperature are visible. These states are basis for further simulation and analysis of hydrostatic testing and working conditions. In upper lower corner of both figures simulated pressure exploitation without and additional steps is presented. Lower three lines of figures present stress state under hydrostatic tests, after release of test pressure and aplication of simulated working pressure, from left to right, for three proposed variants of hydrostatic test pressure. In Figures 7 and 9 view of welded joint traversal cross-section through point of highest residual stress after welding are visible. The location of states is consistent between Figures 5-9.

For S355 steel in all cases after hydrostatic test and during working condition much higher stress level in welded joint is present. This is caused by significant change of elastic limit in weld metal and heat affected zone as an effect of transformation strengthening. In case of 316L austenitic stainless-steel application of significant pressure (simulations 316L_3 and 316L_4) caused equalization of stress level in simulated element. However, this effect was accompanied by significant increase in plastic strain of construction. The level of acceptable deformation can be limited by several factors e.g. previous untreated plastic strain, whether the test is a part of initial verification or periodic maintenance and material platicity. In cases of all tests that result in measurable change in dimensions strain should be monitored [16]. Whereas maximal plastic strain located in the same place as highest stress zone rose only by 0.02% typical plastic strain of pipe surface rose from 0% in case of simulation 316L_1 and 316L_2 to 5% and 7% correspondingly in simulation 316L_3 and 316L_4.

Stress level distribution on cross section of welded joint tells similar story. In S355 cross-section there is visible zone where stress level is significantly higher. This zone is equalized in stress level under hydrostatic test load condition and corresponds to transformation strengthened zone with much higher elastic limit than base material. Moreover any testing pressure resulted in equalization of stress across welded seam depth which is beneficial.

In Figures 8 and 10 plots of combined von Mises stress level for node with highest residual stress after welding for both simulated materials are visible. In case of S355 steel simulation von misses stress level plots shows typical trajectory for welded joint in presence of external forces between 2000 and 2500 seconds when pipe is loaded with pressure boundary condition we see superposition of welding residual stresses and load induced stresses resulting in plastic deformation evidenced by shape of loading curve (no-linear) and drop of residual stress after pressure load condition is released. In case of 316L steel simulation von Mises stress curves in range 2000-2500s have atypical shape. It may be caused by interaction between already strengthened by plastic strain material near welded seam and lack of transformation strengthening.

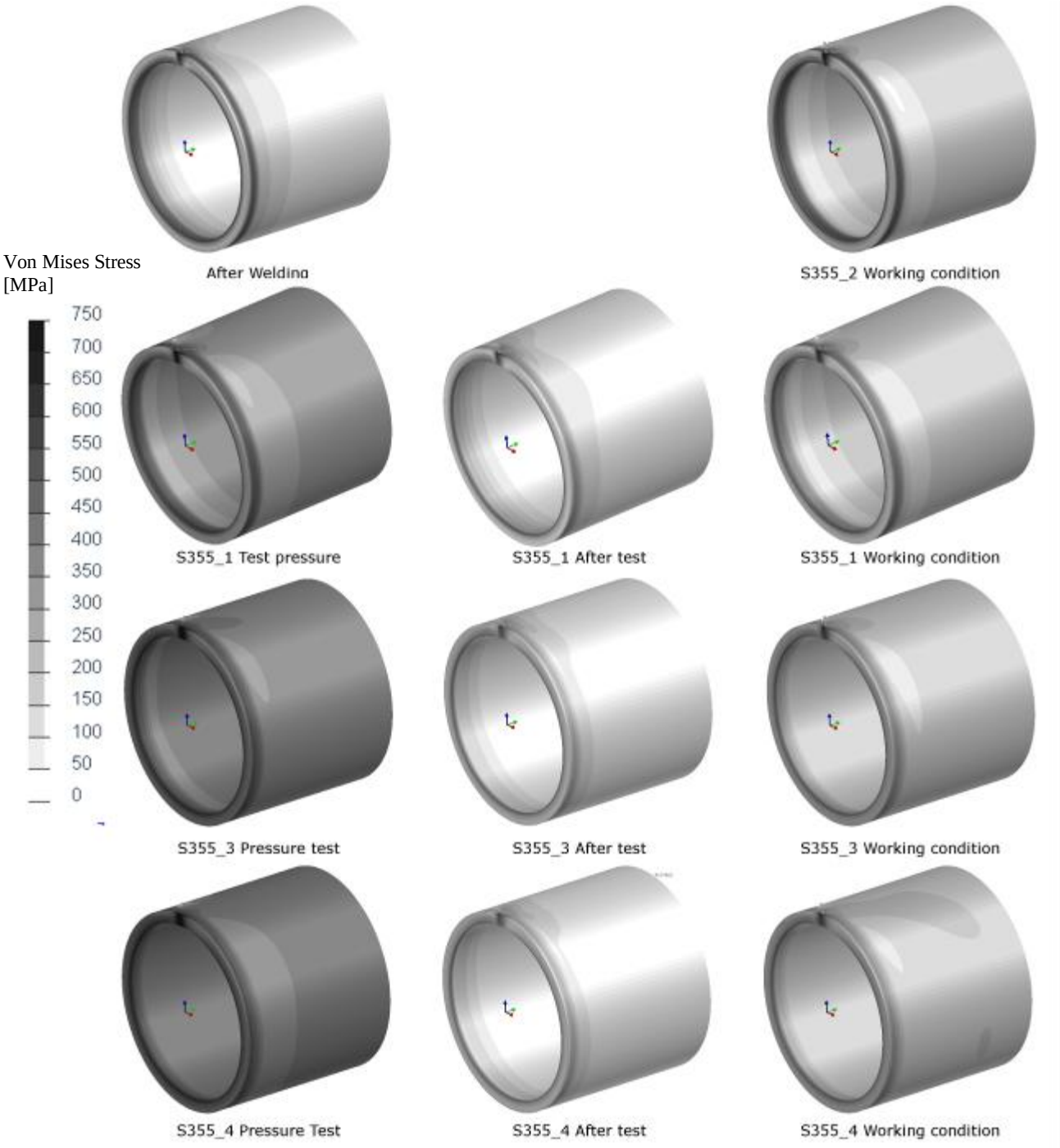

Fig. 5. Von Mises combined stress level for S355 model surface in significant time frames

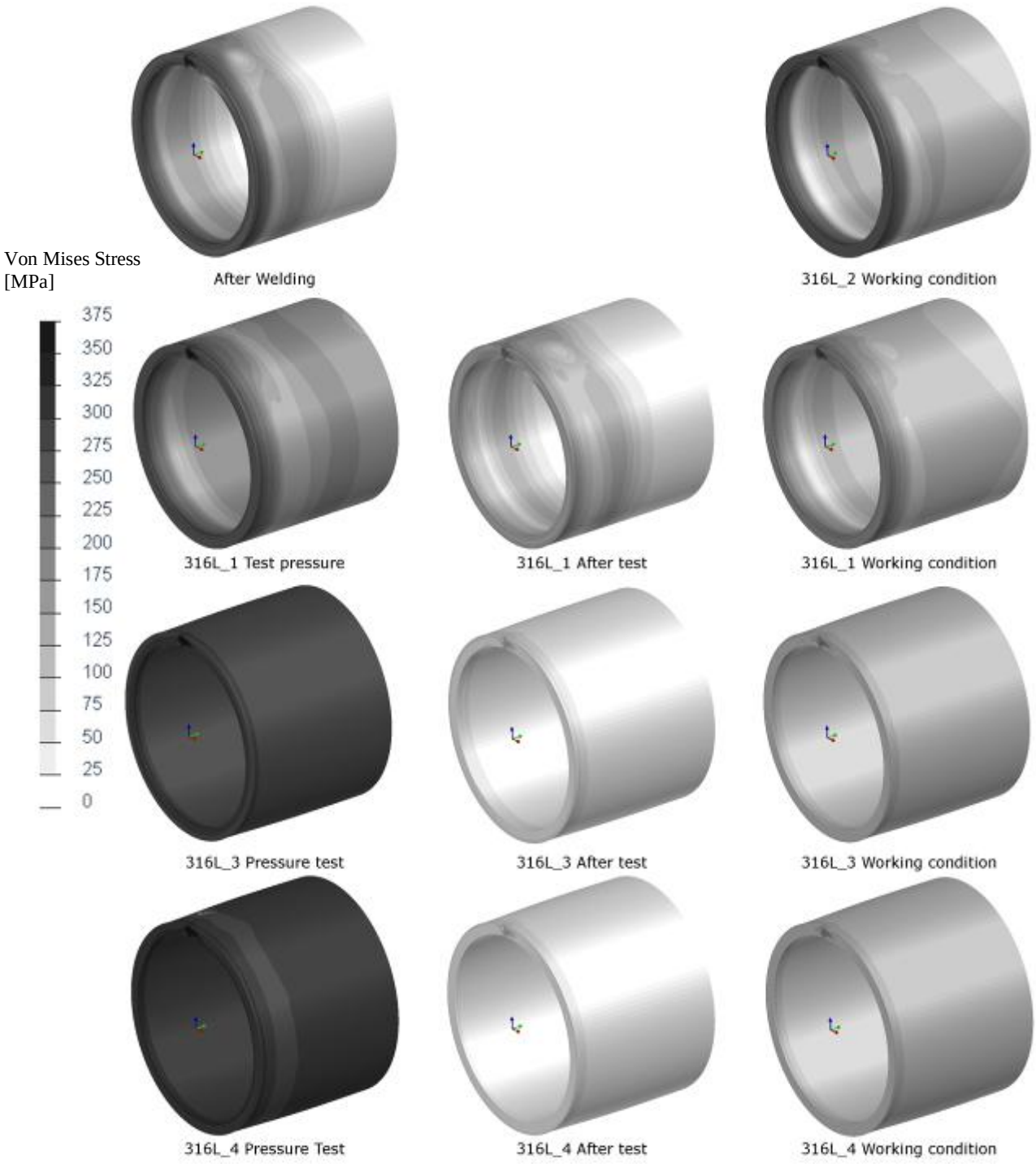

Fig. 6. Von Mises combined stress level for 316L model surface in significant time frames

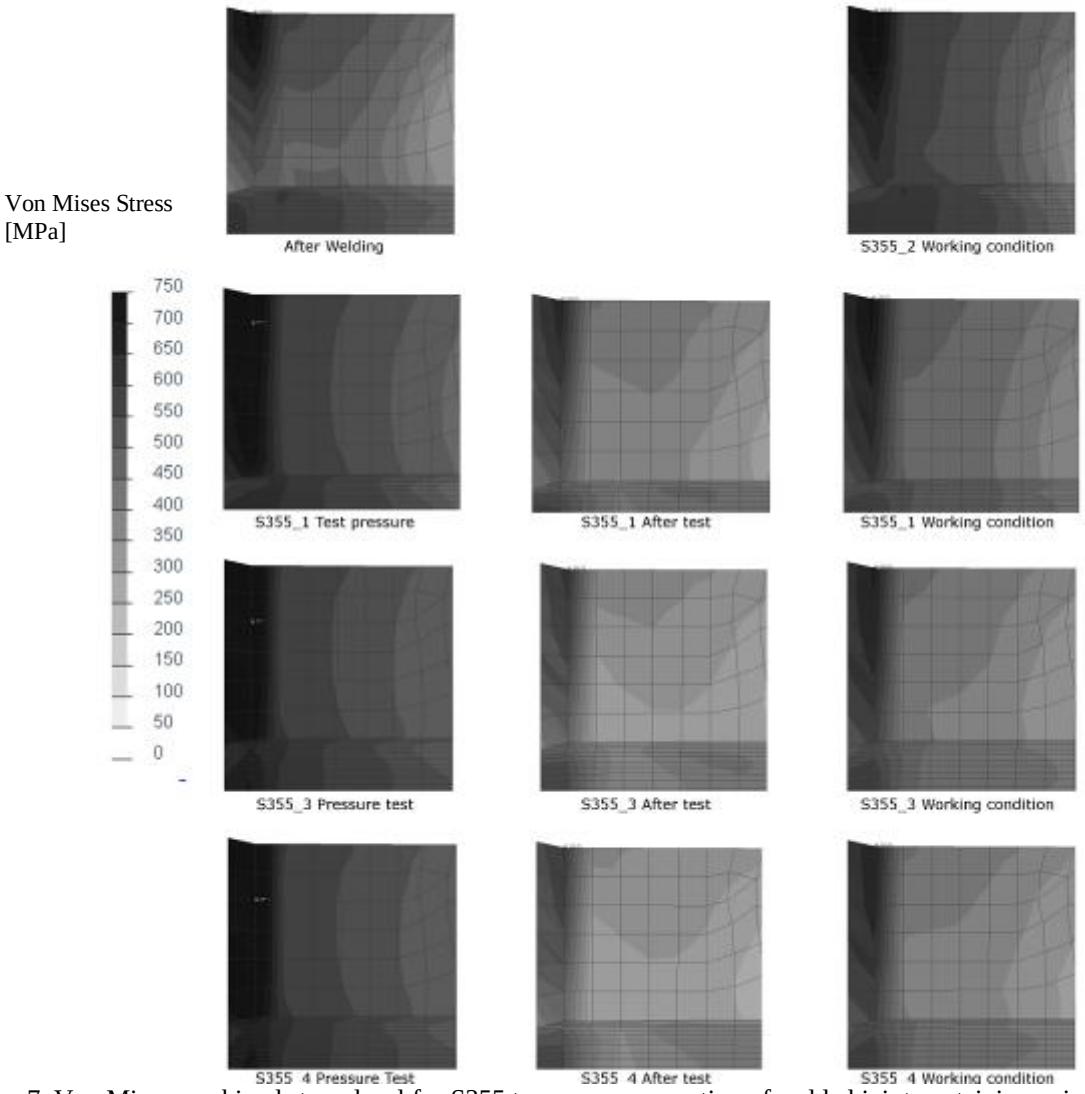

Fig. 7. Von Mises combined stress level for S355 traverse cross-section of welded joint containing point with highest welding residual stresses in significant time frames

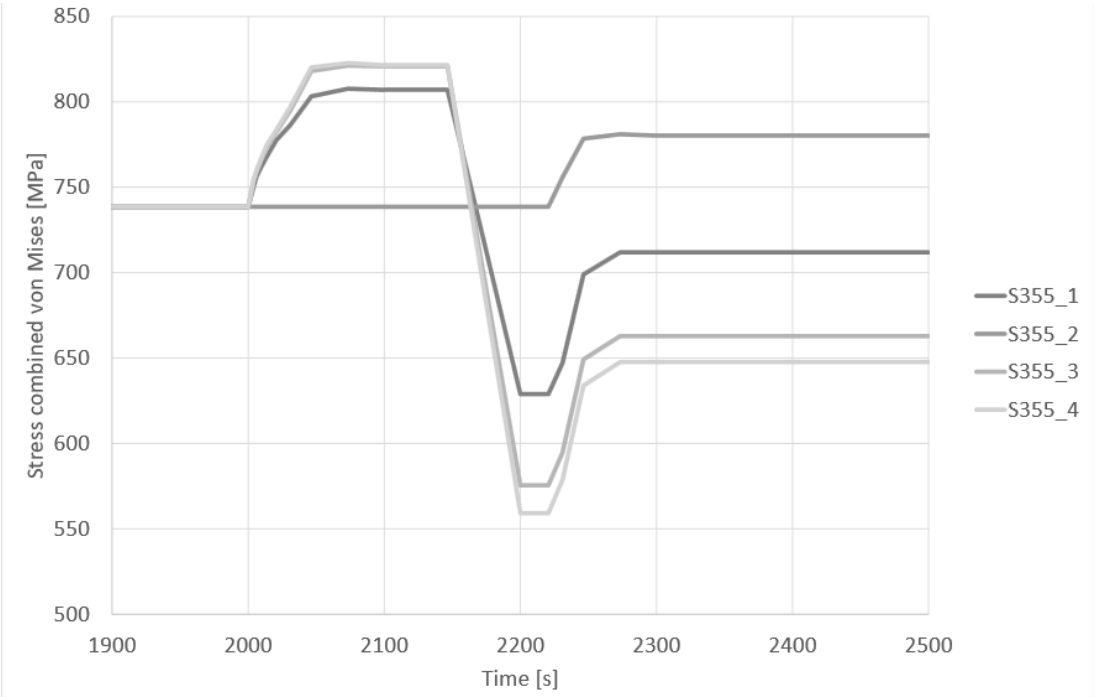

Fig. 8. Time plot of von Mises combined stress for point of highest post weld residual stress in simulation of S355 steel pipes laser welding

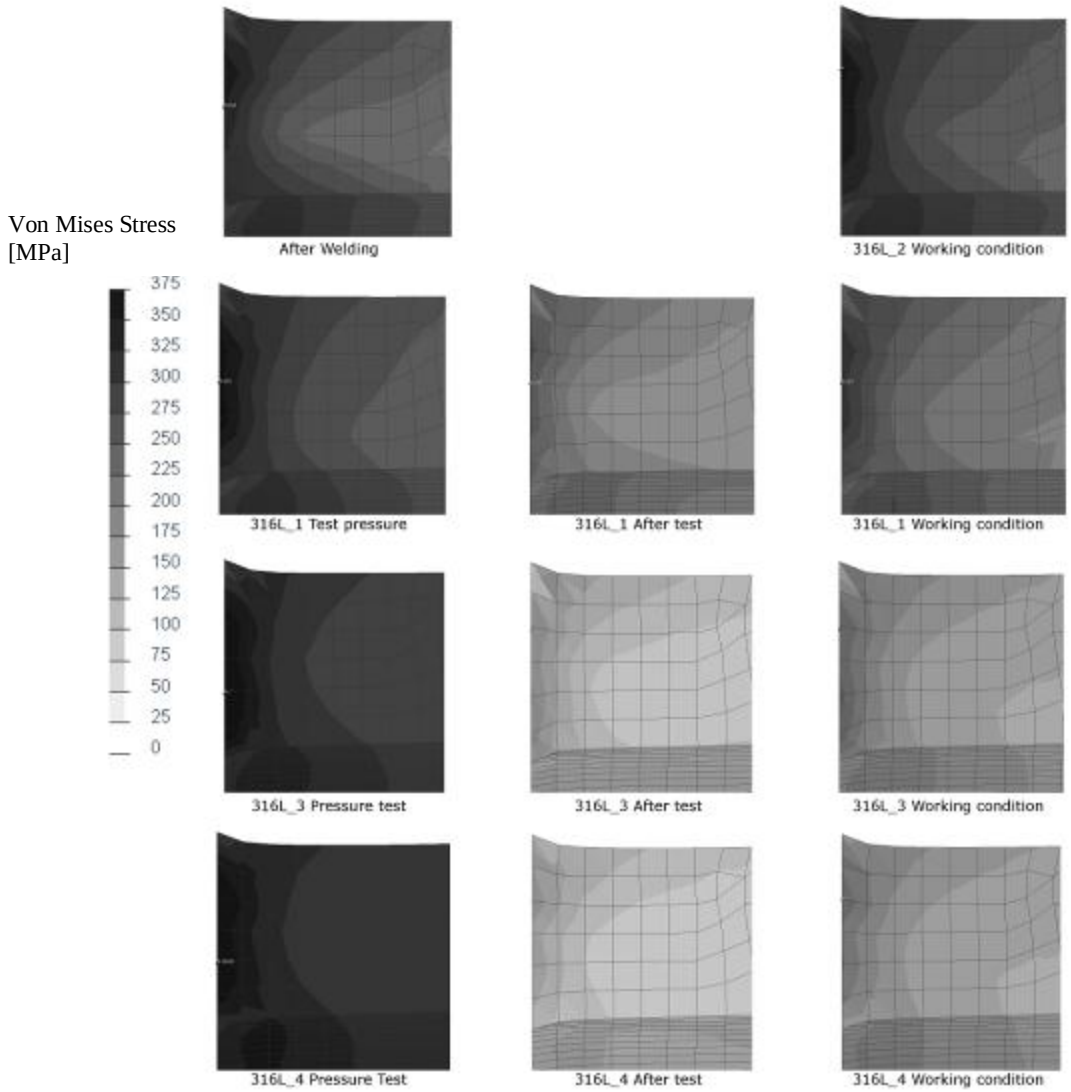

Fig. 9. Von Mises combined stress level for 316L traverse cross-section of welded joint containing point with highest welding residual stresses in significant time frames

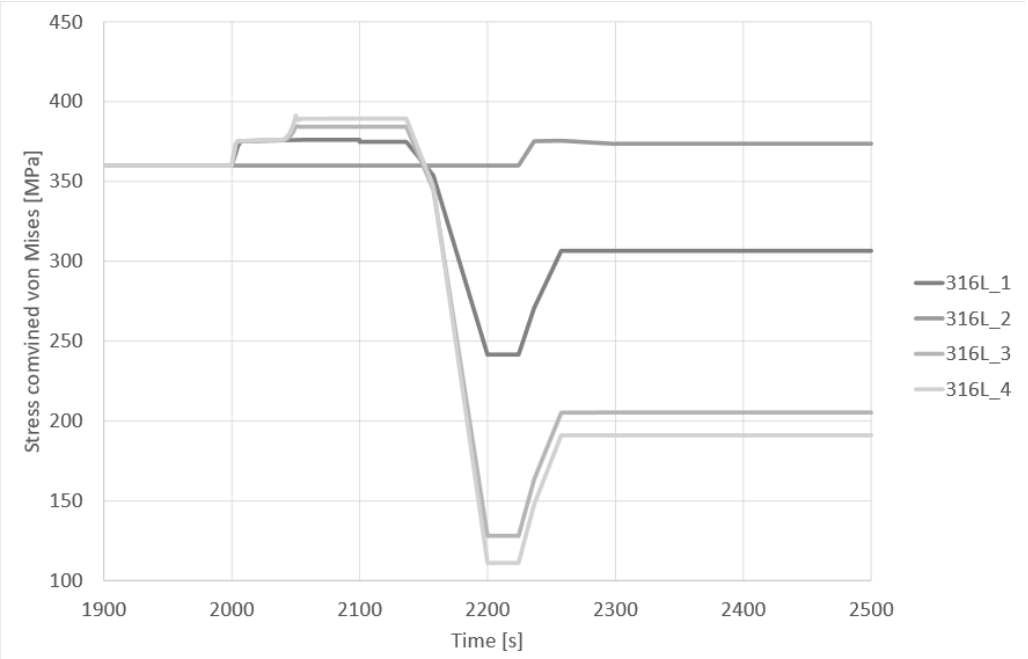

Fig. 10. Time plot of von Mises combined stress for point of highest post weld residual stress in simulation of 316L steel pipes laser welding

4. CONCLUSIONS

In obtained as a simulation result welding residual stress field area with highest stress level is situated near closing of welded seam. This is coincident with engineering practice, evidence by frequent crack formation in this joint area [1]. Application of any overpressure (hydrostatic test with pressure exceeding maximum working pressure) resulted in reduction in simulated residual and working stresses in the weld zone. Working stress level was reduced under level of welding residual stresses in most strained regions in case of hydrostatic test application. Application of higher hydrostatic stress pressure than mandated by DNV Rules and Standards for Classification of Ships Part 4 [15] resulted in further decrease of residual and working stresses. In case of 316L steel application of pressure equal to 105% base material elastic limit reduced level of stress in welded over two times. Relative stress reduction in simulated welded joint of S355 was much lower, due to local transformation hardening in weld metal and HAZ. In materials where welding process causes significant hardening of weld metal and HAZ it is impossible to reach pressure high enough to achieve stress relieving plastic deformation without destruction of elements in unhardened state. The article has proven by means of numeric simulation that hydrostatic testing can be used not only for defect detection, but for lowering and equalization of manufacturing stresses caused by welding.

5. REFERENCES

1. Ahmed, F., *et al.* (2008). *Failure of pipe joints during hydrostatic testing*, Eng. Fail. Anal. **15**, 766–773.

2. Kiefner, J.F., Maxey, W.A., (2000). *The Benefits and Limitations of Hydrostatic Testing*, Available from: http://kiefner.com/wp-content/uploads/2013/05/apihydro.pdf Accesed: 07-01-2020.

3. Novakova, I., Moravec, J., (2016). *Influence of the pressure tanks repeated enameling on the basic material degradation*, MM Sci. J., September, 977-980.

4. Kik T., Moravec J., Nováková I., (2018). *Application of Numerical Simulations on 10GN2MFA Steel Multilayer Welding*. Dynamical Systems in Applications Springer Proceedings in Mathematics & Statistics, **249**, pp. 193-204.

5. Moravec J., Novakova I., Kik T., (2018). *Possibilities of using interlayers during diffusion welding of Ti Gr2 and AISI 316L*, Innovative Technologies in Engineering Production (ITEP'18) MATEC Web of Conferences, 244, art. no. 01013

6. Moravec J., Novakova I., Sobotka J., Kik T., (2018). *Application possibilities of the low-temperature repairs on creep-resistance turbine components from material GX23CrMoV12-1*, Innovative Technologies in Engineering Production (ITEP'18) MATEC Web of Conferences, **244**, art. no. 01017.

7. Devaux, J. *et al.* (2000). *Numerical study of the plastic behaviour of a low alloy steel during phase transformation*, Proc. Of 1st Int. Conf. On Thermal Process Modelling and Computer Simulation, J. of Shanghai Jiaotong University, **E-5**(1), 206-212.

8. Moravec, J., Kik, T., Novakova, I., (2016). *Application of numerical simulations on X10CrWMoVNb9-2 steel multilayer welding*, MM Sci. J., November, 1190-1193.

9. Kik, T., *et al.* (2017). *New method of processing heat treatment experiments with numerical simulation support*, ModTech International Conference IOP Conference Series: Materials Science and Engineering, **227**(2017), 012069, doi:10.1088/1757-899X/227/1/012069.

10. Giętka, T., *et al.* (2016). *Numerical Simulation of Duplex Steel Multipass Welding*, Arch. of Metall. and Mater., **61**(4), 1975-1984.

11. Vanek, M., *et al.* (2016). *Improvement of model of aluminium alloys behaviour for application in numerical simulations of welding*, MM Sci. J., November, 1370-1375.

12. Welding simulation user guide, Sysweld manual 2016 ESI Group, Available from: https://myesi.esi-group.com/downloads/software-documentation/sysweld-2010-example-manual-pdf Accessed: 03-05-2020.

13. Wu, W., *et al.* (2006). *Numerical investigation on laser transformation hardening with different temporal pulse shapes*, Surf. & Coat. Technol., **200**, 2686–2694.

14. Goldak J., et al. (1996). *Thermal stress analysis in welds for hot cracking*. Proceeding of the 1996 ASME PVP Conf., pp. 1-26, ASME, Pressure Vessels and Piping Division PVP, Montreal

15. DNV GL rules for classification: Ships (RU-SHIP) Available from: https://rules.dnvgl.com/ServiceDocuments/dnvgl/#!/industry/1/Maritime/`111/DNV%20GL%20rules%20for%20classification:%20Ships%20(RU-SHIP) Accessed: 07-12-2019.

16. Kiefner, J. F., Maxery, W.A., (2014). *Hydrostaic Testing*, Pipeline Rules of Thumb Handbook, McAllister, E.W. (Ed), pp. 150-172, Gulf Professional Publishing, USA (Waltham).

Received: September 16, 2020 / Accepted: December 15, 2020 / Paper available online: December 20, 2020